ACS APPLIED MATERIALS & INTERFACES

www.acsami.org

Research Article

Multifunctional Untethered Soft Machines Driven by 4D Printed Electrically Responsive Actuators

Yuliang Xia,[†] Tong Mu,[†] Jianglong Guo,* Yanju Liu, and Jinsong Leng*

Cite This: *ACS Appl. Mater. Interfaces* 2025, 17, 36059−36068

Read Online

ACCESS | Metrics & More | Article Recommendations | Supporting Information

ABSTRACT: Untethered robots, compared with their tethered counterparts, may bring enhanced autonomy. It is highly desirable to engineer multifunctional, lightweight, rapid, and low-voltage driven untethered soft robots that have enhanced adaptability and safer interaction capabilities. Here we present an untethered soft robot by a smart integration of 4D printed liquid crystalline elastomer (LCE) actuators with the associated electronics. The LCE artificial muscle, which consists of a modified LCE sandwiched between a polyimide based heating film and a silicone adhesive, not only has adjustable transition temperatures (39−46 °C) and modulus (0.61−2.57 MPa) but also has decent mechanical properties such as adequate rigidity to support certain loads and sufficient propulsive forces (13.7 MPa) to facilitate robotics motions. As a result, we developed an untethered, compact LCE soft robot that is the lightest (overall weight of 9.87g) and the quickest (0.28 body length per minute), and has the lowest cost of transportation (CoT of 7), among all untethered electric-driven LCE robots. The LCE robot can also be used for grasping and demonstrating obstacle crossing capability on challenging terrains.

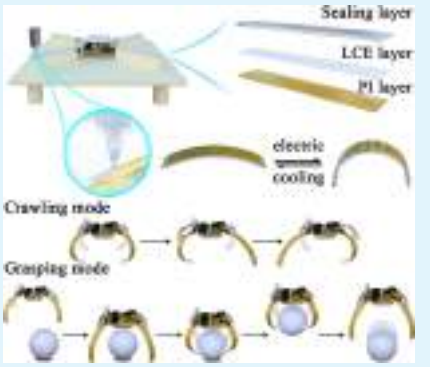

KEYWORDS: *4D printing, liquid crystalline elastomer actuator, untethered soft robotics, soft crawling, soft grasping*

1. INTRODUCTION

Untethered robots, which usually use on-board power sources, are highly important to complete long-range autonomous missions[1−3] that require larger ranges of mobility, and are more suitable for realizing tasks in challenging spaces such as narrow pipelines.[4−6] Untethered soft robots, compared to their rigid counterparts, have enhanced dexterity (due to higher degrees of freedom), increased robustness, and safer interaction capabilities and are thus more applicable to adaptive and complex tasks in unpredictable and unstructured environments[7−12] such as forests and ruins (see Figure 1A).

Soft actuators are key components of untethered soft machines.[12−16] Pneumatic actuators,[17,18] magnetic actuators,[19] dielectric elastomer actuators,[1] ionic polymer−metal composite actuators,[20] and shape memory actuators[21] have been used to develop various untethered soft robots. Pneumatic methods offer robust actuation capabilities but often require cumbersome, energy-intensive pumps. Consequently, they might not be the first choice for compact, lightweight, untethered soft robots.[18] Magnetic approaches present lightweight solutions for untethered soft robotics. Yet, their reliance on specialized external magnetic fields can complicate control, especially when rapid movements are involved.[19] Dielectric elastomer actuators provide the advantage of simpler controls and energy efficiency; but the need for high voltages can raise safety concerns.[1] Ionic polymer−metal composite actuators operate at low voltages, though they might not provide the strongest force outputs.[20] While shape memory actuators can be used to deliver powerful actuations, they pose challenges in precision control and scalability for mass production.[22−25]

Liquid crystalline elastomer (LCE) actuators can be used to offer fully soft, relatively powerful, robust, and muscle-like actuations[26,27] which can be triggered by several stimuli including light,[28] heat,[29] magnetic fields,[30,31] and electricity.[32] LCE actuators driven soft robots can bring a class of untethered soft robots that can be operated using low voltages and thus can be lightweight[33] and portable (see Figure 1A). Light,[34] magnetic field,[30] and heat responsive[29] LCE actuators all require external stimulus fields, significantly limiting their moving ranges, but this limitation can be addressed by electric responsive LCE actuators. It is, however, still relatively challenging to design and develop electric responsive LCE actuator driven untethered soft robots.

The successful fabrication of LCE actuators requires delicate control over their deformations across varying temperature ranges. However, the design of LCE robots entails the consideration of several factors; for instance, excessively high or low driving temperatures are not conducive to creating LCE robots. A low transition temperature could transform the

Received: March 27, 2025
Revised: May 26, 2025
Accepted: May 27, 2025
Published: June 6, 2025

https://doi.org/10.1021/acsami.5c06159
ACS Appl. Mater. Interfaces 2025, 17, 36059−36068

Figure 1. Electrically responsive LCE actuator driven multifunctional untethered soft machines. (A) Portable untethered soft machines can be conveniently used for search and rescue tasks in unstructured environments. (B) Multifunctional untethered soft robot fabrication strategy. (C) The electrically responsive LCE actuator driven untethered soft robot walking on a plastic table with a speed of 0.28 body length per minute. (D) The electrically responsive LCE actuator driven untethered soft gripper grasping a table tennis of 2.7 g. Body length = 5.96 cm. Scale bars = 2 cm.

actuator into an isotropic state at room temperature, inhibiting deformation upon heating. Conversely, a high transition temperature could trigger the LCE's failure or detachment from other robot parts, leading to considerable energy loss.[35] Therefore, designing an appropriate LCE actuator is a challenging task. Moreover, the preparation of LCE actuators often involves vacuum and heating steps in the synthesis process, usually extending over 2−3 days, notably longer than the preparation of other material-based soft robots.[36,37]

https://doi.org/10.1021/acsami.5c06159
ACS Appl. Mater. Interfaces 2025, 17, 36059−36068

Table 1. Comparison of the Main LCE Actuator Driven Soft Robots

untethered/tethered	stimulus methods	total robot weight (g)	maximum moving speed (body length/min)	loading capability (g)	cost of transport (CoT)	function			ref
						crawling	loading	grasping	
untethered	electricity	N/A	0.05	N/A	50000−100000	yes	yes	yes	He et al.[36]
untethered	electricity	54.20	0.11	N/A	2985−27000	yes	no	no	Boothby et al.[37]
untethered	heat	N/A	2.53	N/A	N/A	yes	no	no	Kotikian et al.[29]
untethered	light	0.02	1.50	0.01	N/A	yes	no	no	Pilz da Cunha et al.[10]
tethered	electricity	N/A	0.09	N/A	N/A	yes	no	no	Wang et al.[46]
tethered	electricity	N/A	0.05	N/A	N/A	yes	no	no	Song et al.[49]
untethered	electricity	9.87	0.28	6	7−54	yes	yes	yes	this work

Beyond material-related issues, another challenge lies in applying actuators to robots under conditions closely mimicking real environments. Most previous studies employing LCE actuators utilized a simplistic inchworm robot mode to facilitate crawling; however, these actuators lack the necessary rigidity to uphold the robot's structure. Therefore, the robot is restricted to $x-y$ plane motion, giving the appearance of the actuator dragging the robot. In real-world scenarios, robotic legs resembling those of insects, such as spiders, are desirable, ensuring light weight, adequate rigidity, and deformability.[38,39] Furthermore, heating the actuator can lead to the separation of the LCE and the heating layer due to the absence of a robust chemical bond or physical interaction between them. This issue is particularly pronounced when the heating layer exhibits a high stiffness.

In this paper, we present a novel approach to creating untethered soft robots by integrating LCE bending actuators with the associated electronics through 4D printing. 4D-printing is a process by which an object printed in 3D transforms into a different structure, based on external energy, such as temperature or light or other stimuli in the environment. 4D printing can be used to easily produce complex and multidirectional actuations through customized printing trajectories.[40−42] Small-scale superlightweight LCE actuators[43,44] can thus be achieved. In addition, 4D printing methods with multimaterial and multiscale structures can be used to make robots that transform from flat sheets with built-in electronic devices into multifunctional machines in an autonomous manner (see Figure 1B).

In this study, we utilized a chain extender, hitherto unexplored in prior research, to adjust the transition temperature (39−46 °C) and storage modulus (0.61−2.57 MPa) of the LCE. Leveraging LCE materials with optimal transition temperatures, we designed, manufactured, and characterized a novel bending LCE actuator. The actuator has a three-layer composition, i.e., a polyimide (PI) heating film, an LCE actuator layer, and a silicone glue sealing layer. This configuration, with its lightweight properties, ensured that the actuator can maintain optimal mobility while providing the requisite rigidity to support the robot's structure. Moreover, the encapsulation of the LCE and the heating film by the silicone glue prevents potential separation issues. Such issues could arise from differential deformation rates between the LCE and the PI heating films during LCE deformation, and the encapsulation strategy effectively mitigates this risk. We also developed an FEM simulation model to verify the effectiveness of structural design and motion control.

As a result, we designed and fabricated an untethered, compact LCE robot that is the lightest (overall weight of 9.87 g, ≈6 times lighter) and the quickest (0.28 body length per minute, ≈2.5 times faster) and has the lowest cost of transportation (CoT) of 7 (≈400 times lower), among all untethered electric-driven LCE robots (Figure 1C; see Table 1 for comparison). The robot can also be used to act as a soft gripper (see Figure 1D) that can adaptively lift irregular masses (weight over 14.55 g, ≈1.5 times its own weight). In addition, the multifunctional untethered LCE robot demonstrated an obstacle crossing capability on challenging terrains. This work offers a new LCE actuator manufacturing approach and provides an integrated flexible robot design and fabrication strategy toward multifunctional untethered soft machines that may find useful applications in unmanned inspections and detections in complex and unstructured environments such as ruins and forests.

2. MATERIALS AND METHODS

2.1. Materials. The liquid crystal acrylate RM82 (LC monomer, HCCH Company), RM257 (LC monomer, HCCH Company), thiol chain extender 1,5-pentanedithiol (Sigma-Aldrich), cross-linker triallyl isocyanurate (TAIC), antioxidant butylhydroxytoluene (BHT, Sigma-Aldrich), photocuring agent (2-hydroxyethoxy)-2-methylpropiophenone (HHMP, Sigma-Aldrich), triethylamine (catalyst, Sigma-Aldrich), silicone glue (PH8860, Pinheng Company), and the polyimide electric heating films were all commercially purchased.

2.2. Preparation of the LC Oligomer. RM82 (2.038g), RM257 (0.594g), thiol chain extender (0.7097 g,), TAIC (0.2543g), antioxidant BHT (0.072g), and photoinitiator HHMP (0.054g) were mixed in a 10 mL stainless steel cartridge and heated at 90 °C for 30 min, and the molten solution was formed. The catalysis TEA (0.036g) was then added into the solution which was mixed 30 s and heated at 60 °C 2h to ensure that the thiol was fully reacted with the acrylate. Eventually, printable polydomain LC oligomer ink was obtained after the reaction (for composition detail see Table S1).

2.3. Preparation of the LCE Artificial Muscles. The LC oligomer ink was afterward loaded into a high temperature extruder printing head which was an attached device of the direct-ink printer (3D Bioplotter, EnvisionTEC). The LC oligomer ink was printed at 65 °C with 1 bar pressure and was printed on the PI heating film in parallel condition directly. Those oligomers were cross-linked posterior to the printing via persistent irradiation from 365 nm LEDs at 0.8 mW cm^{-2}. After that, the LCE artificial muscles were postcured with 365 nm UV light for 20 min.

2.4. Preparation of the LCE Actuators. To fabricate LCE actuators, the PI heating film was prestretched into a semicircle structure. The PI heating film was then placed under the direct-ink printer and laid flatly. Next, the LCE and PI heating films were encapsulated by printing silicone glue on the LCE to form an actuator. After the actuator was postprocessed, it was placed in the air for 2 h to cure the structural adhesive, after which it was removed from the direct-ink printer to obtain a curved LCE actuator.

2.5. Preparation of the Untethered Robot. To produce an untethered robot, four PI heating films and a microcontroller were placed on the direct-ink printer. The preparation process of PI heating film can be seen in Figure S12. The LCE and structure glue were

https://doi.org/10.1021/acsami.5c06159
ACS Appl. Mater. Interfaces 2025, 17, 36059−36068

directly printed on the PI heating film set, and the connection between the leg and the microcontroller was determined according to the program. When the material was fully cured, the actuator and microcomputer could be combined to form a flexible robot with multiple functions. We fixed 4 prepared LCE actuators to the PI plate and regulated the actuators via single-chip microcontroller (3.7 V). A 3.7 V battery (uxcellDC, 100 mAh) was utilized as the power source (for details of weight see Table S2).

2.6. Characterizations. A PerkinElmer Spectrum Two Fourier transform infrared (FT-IR) spectrometry detector was afterward utilized to explore the specimens via production of FT-IR spectra via the attenuated total reflectance approach. The anisotropic alignment of the sample was characterized by a 2D-WAXD experiment conducted on a Xeuss 2.0 diffractometer with a Pilatus 300 K detector in Line Eraser mode. DMA assays were completed in tension mode via a DMA Q800 instrument (TA apparatus). DSC measuring (DSC 1 STAR Device, Mettler-Toledo) was completed in a N_2 environment. The samples were first heated from 25 to 130 °C and afterward cooled to 25 °C at 10 °C/min. The thermostability of the LCE samples was tested via TGA (TGA/DSC 1 STAR Device, Mettler-Toledo) with specimens heated from 25 to 500 °C at 10 °C/min in a N_2 environment. The superficial temperature of LCE actuators in actuation was identified via heat imaging technology (JENOPTIK InfraTec). The transformation behaviors of the LCE artificial muscles, LCE actuators, and multifunctional untethered LCE soft robots were captured with a digital camera.

3. RESULTS AND DISCUSSIOS

3.1. LCE Artificial Muscle Design, Fabrication, and Characterization. In order to design and fabricate LCE artificial muscle materials with adjustable actuation temperature and mechanical properties, we employed 4D printing (which can be used to produce smaller, lighter LCE actuators) and a two-step cross-linking method. Figure 2A presents the schematic of printing LCE artificial muscles with tailored thermal mechanical performances. Initial formulation of nematic oligomer inks involved a blend of LC mesogens and an isotropic dithiol 1,5-Pentanedithiol. This facilitated the thiol−acrylate Michael addition reaction, creating a printable ink. During printing, the ink involving non-cross-linked LC oligomers was initially heated up to 65 °C to ensure the oligomer has sufficient liquidity. Afterward, the LC oligomers were extruded via the nozzle of a direct-ink printing machine (3D Bioplotter, EnvisionTEC). Nematic inks with thiol terminations can be printed directly. This printing procedure regionally programmed the mesogen alignment orientation along the printing path through the shear stress.[45] Subsequently, the ink was photo-cross-linked via the reaction between the thiol-terminated LC oligomer and the trifunction vinyl cross-linker triallyl isocyanurate (TAIC). Fourier transform infrared spectroscopy (FT-IR) was utilized to make sure that the thiol−acrylate reaction was complete (Figure S1).

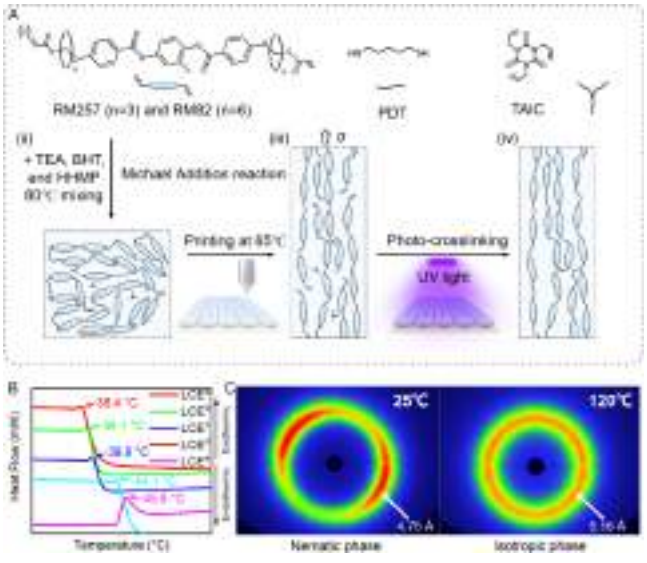

Figure 2. LCE artificial muscle chemical components, fabrication process, and actuation performance. (A) RM257 and RM82 work as the LC mesogen, 1,5-pentanedithiol works as the chain extender, and TAIC works as the cross-linker (i). Polydomain LC oligomer could be acquired via heating the above mixtures (ii). The monodomain LCE has been obtained by printing the LC oligomer (iii) with UV irradiated to produce the second cross-linking process (iv). (B) T_{NI} of LCE from 38.4 to 45.8 °C with different moiety ratios. The results were conducted by DSC characterization. (C) 2D-XRD patterns of LCE under 25 and 120 °C. The LCE demonstrates nematic phase at 25 °C and isotropic phase at 120 °C, resulting in reversible transformation.

The experimental methodology revealed certain issues associated with the use of (2,2′-(ethylenedioxy)diethanethiol (EDDET) or 1,3-propanedithiol (PDT) as molecular chain extenders. When EDDET was employed as the extender, the high molecular weight resulted in a reduced transition temperature for the material, and the LCE easily transforms directly into isotropic state at room temperature, subsequently impeding adequate deformations upon heating. Conversely, using PDT as the extender resulted in an excessively high transition temperature, creating difficulties for the actuator in terms of printability and deformability.[45] Consequently, we opted for 1,5-pentanedithiol as the extender, a choice motivated by its intermediary molecular weight between EDDET and PDT. The use of 1,5-pentanedithiol as a chain extender has not been previously reported in the literature for 4D printed LCEs. This choice allowed us to fine-tune the nematic−isotropic transition temperature (T_{NI}), thereby controlling the actuation temperature of the cross-linked LCE.

The results of thermal characterization are presented in Figure S2. By manipulating the ratio between RM82 and RM257 (specific material ratios can be seen in Supporting Infomation Table S1), we can control the T_{NI} of LCE within 39−46 °C. (Figure 2B and Figure S2A). The degradational temperature of LCE was about 358 °C which was remarkably greater in contrast to the T_{NI} ensuring the steady heat actuation of LCE actuators (Figure S2B). Dynamic mechanical analysis (DMA) test has been adopted for examining the mechanical properties of LCEs with different molar ratios (Figures S3 and S4). LCE with solely RM82 exhibited an optimal elastic modulus (2.57 MPa) and a lower loss factor (0.30). Therefore, LCE^e was used as the main research material in subsequent experiments.

To guarantee the LCE's reversible deformability, we characterized the orientation of the mesogen unit on a microscopic level. The Debye ring in 2D wide-angle X-ray diffraction (2D-WAXD) can be used to determine the direction of X-ray diffraction within a material, providing insight into the microscopic orientation of the samples. Its shape and symmetry can be used to assess this orientation with satisfactory accuracy. Here, the monodomain LCE exhibited a uniaxial direction along the direction of mechanic stretch by characterizing with 2D-WAXD features, where the nematic ring varied to two transvers arcs. These results proved that the LCE presented a uniaxial direction along the direction of the mechanic stretch. Especially, the reflection at 2θ = 18.64° was obvious, which was in correspondence to a d-spacing of approximately 4.75 Å (Figures S5 and S6). When the temperature increased to 120 °C, the

https://doi.org/10.1021/acsami.5c06159
ACS Appl. Mater. Interfaces 2025, 17, 36059−36068

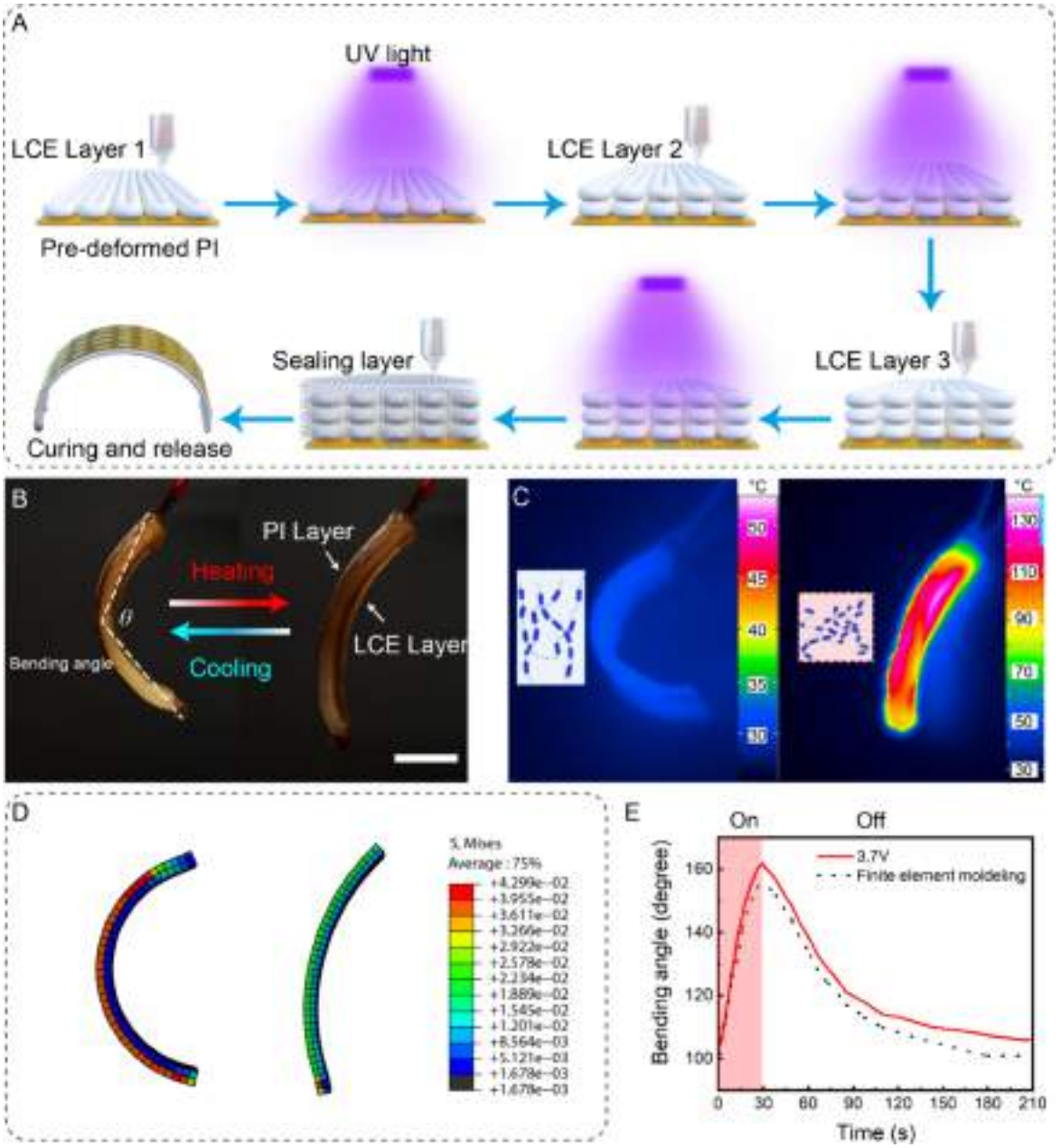

Figure 3. LCE bending actuator fabrication, characterization, and simulation. (A) Fabrication process of the LCE actuator. A predeformed PI heating film was placed on the printing bed according to design requirements. Three layers of LCE material were then printed on the PI heating film with subsequent UV curing. The sealing layer consisting of silicone glues was printed afterward to combine the LCE and heating film together. Finally, after taking off the LCE actuator, the PI heating film returned to its original curved shape (97.3°). (B) The morphing process of the LCE actuator. The left is the original shape (105.94°), and the right is the morphed shape (162.00°). (C) The temperature distribution of the LCE actuator during transformation. As temperature rises, the actuator contracts according to the molecular contraction (see right). The actuator reverts to the original state (see left) during the cooling process because of the rearrangement of liquid crystal molecules. (D) FEA modeling result of the configurations shows stress distributions within the LCE actuator as a function of different temperatures. (E) Comparison between simulation and experimental results of LCE actuator bending under 3.7 V. Scale bar = 1 cm.

temperature was higher than the T_{NI} of the sample, so that the liquid crystal LC mesogen lost its orientation, and 2D-XRD showed a regular nonoriented ring at this time (Figure 2C).

Last, we examined the reversible morphing behavior of pure LCE materials under varied conditions. In order to quantify the transformation behaviors of the LCE artificial muscles, the actuation strain was defined as $\varepsilon = [(l_0 - l)/l_0] \times 100\%$. When the initial and actuated states of the LCE artificial muscle are presented, l_0 and l are the lengths of the muscle, respectively. This artificial muscle (460 mg) can lift a load of 490 N with an actuation strain of 42.6% (Figure S7 and Movie S1) upon heating with a heat gun with 120 °C. Thermodynamic cycling experiments based on LCE artificial muscles were carried out to test the recoverable deformation rate of LCE at high and low temperatures. The results showed that the LCE artificial muscle could produce reliable reversible deformation between 25 and 150 °C, validating its potential use as an actuator for electrically driven untethered soft robots (Figure S8).

3.2. Electricity Controlled LCE Actuator Design, Fabrication, and Characterization. To render the actuator

https://doi.org/10.1021/acsami.5c06159
ACS Appl. Mater. Interfaces 2025, 17, 36059−36068

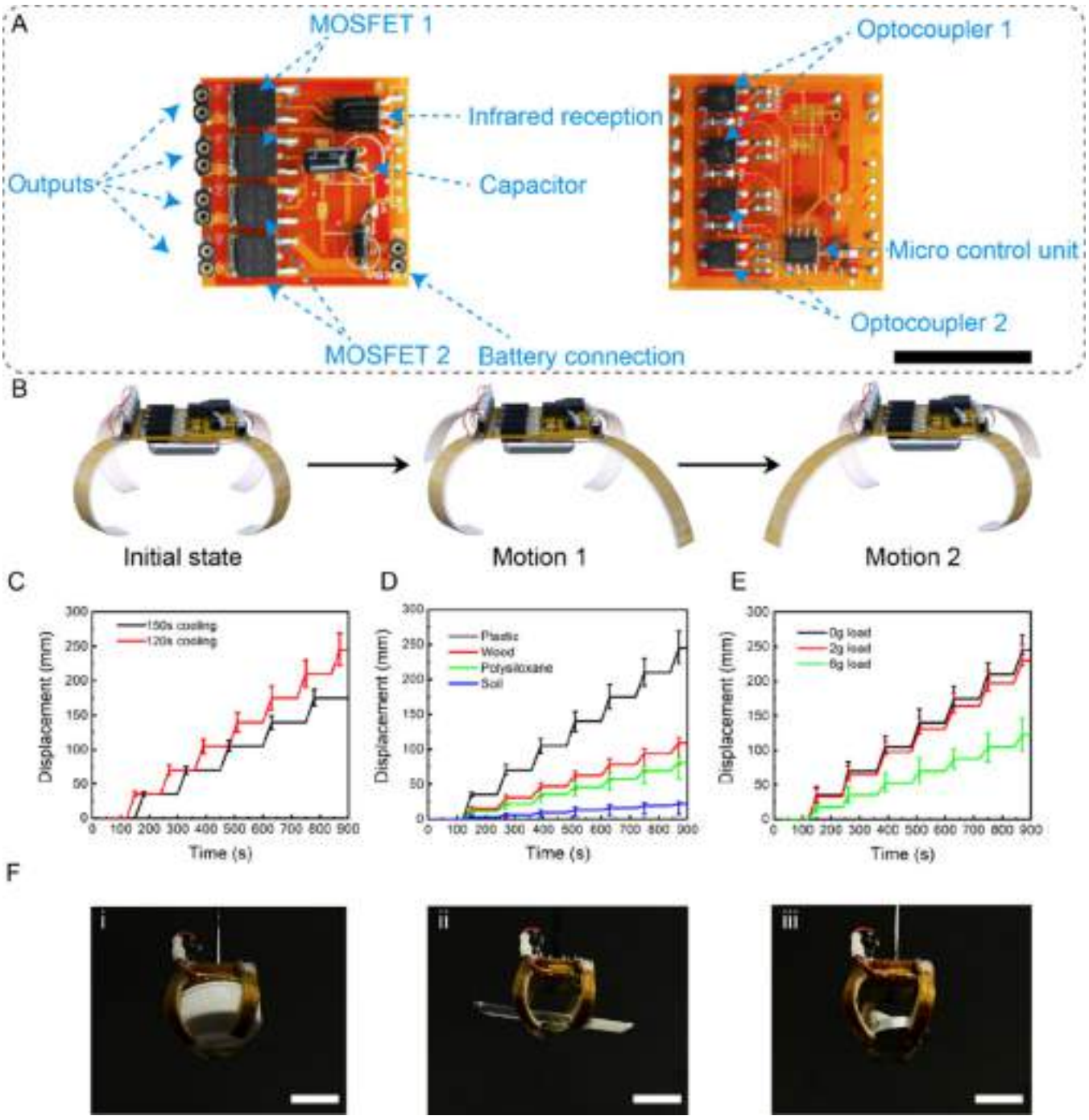

Figure 4. LCE actuator driven untethered soft robots. (A) Robot hardware. The left is the top view of the printed circuit board, and the right is the bottom view. The battery and connections lines are omitted here. (B) Rendering schematic diagram of the LCE robot motion process. (C) Displacements of the untethered robot using different cooling times on plastic. (D) Displacements of the untethered robot on different crawling surfaces. (E) Displacements of the untethered robot under different loading weights on plastic. (F) Grasping different objects including (i) a bottle cap of 2.23 g, (ii) a glass slice of 4.86 g, and (iii) a metal cap of 14.55 g. Scale bar = 2 cm.

that can be more functional in applications, it is desirable to retain the deformability of the LCE actuator significantly while ensuring sufficient rigidity to support the robot's weight. Previous reports on LCE actuator structures highlight a trade-off between low weight and reduced stiffness. This deficiency means that the actuator can only facilitate planar movement of the robot, rather than sustaining the robot's weight as an insect's legs would.[46] This limitation restricts the mobility modes of the LCE robot. Traditional printing schemes also face the challenge of the LCE deforming upon heating; the weak interaction between the LCE and the PI heating film often leads to separation and, subsequently, structural failure.

To overcome these issues, we developed an electrically triggered LCE actuator by introducing a supportive layer (polyimide heating film) and a sealing layer (silicone glue) utilizing 4D printing technology (Figure 3A). The actuating LCE layer is initially printed on the polyimide heating film, followed by the application of the silicone glue layer. Under its

https://doi.org/10.1021/acsami.5c06159
ACS Appl. Mater. Interfaces 2025, 17, 36059−36068

own weight, the silicone glue wraps the LCE, flowing downward to contact the PI heating film. After a 2 h solidification period, the LCE is securely sealed within the actuator assembly. The integration of the PI heating film and silicone glue ensures the actuator maintains requisite rigidity to support the robot. Concurrently, the silicone glue encapsulates and affixes the LCE to the PI heating film, ensuring a tight connection during deformation and preventing failure during heating.

Subsequently, we characterized the actuating performance of the LCE actuator (see Figure 3B and Movie S2). We defined θ as the bending angle for the LCE actuator (formed by connecting the two ends of the actuator and the middle point). We utilized 3.7 V as the main voltage to make general-purpose LCE actuators. A maximum bending angle as θ = 162.00° was observed after 30 s electricity heating. The θ of the LCE actuator can return to 105.94 ° after 2 min cooling. The actuator achieves its maximum bending angle (162.00°) within 30 s of applying 3.7 V and returns to its original state (105.94°) within 2 min upon voltage removal, as detailed in Figure 3C. The heat imaging results, captured by JENOPTIK (InfraTec), displayed the superficial temperature of LCE actuator membrane in the course of heating under 3.7 V. The greatest superficial temperature elevated from 25 to 130 °C in 30 s (Figure S9). While turning off the voltage, the LCE actuator temperature progressively reduced to the ambient temperature, and the LCE actuator restored to the initial morphology in 4 min. This phenomenon stemmed from the fact that the heated side of the LCE tended to shrink and deform when it was heated and the fact that the side closer to the heat source had a greater deformation ability. A detailed comparison between the stretching actuator and bending actuator has been presented in Supplementary Text 1. Furthermore, this multilayer design also isolates the LCE from its surroundings, allowing for enhanced resistance to environmental pollution, extended service life, and reduced energy consumption.

Figure 3D represents the quantitative finite element analysis (FEA) modeling result for the LCE actuator during the cycle of reversible shape-transforming (for the specific method applied in the model, see Supplementary Text 2). We implemented a constitutive model in Abaqus to simulate the mechanical behavior of the LCECs. The model utilizes a piecewise linear elastic modulus to differentiate between the nematic and isotropic phases of the material. Specifically, distinct linear elastic properties are defined for each phase:

$$E = \begin{cases} E_{0,\mathrm{n}} - a_{\mathrm{n}}T, & T \le T_{\mathrm{trans}} \quad (1) \\ E_{0,\mathrm{i}} - a_{\mathrm{i}}T, & T > T_{\mathrm{trans}} \quad (2) \end{cases}$$

Here, the subscript n denotes the nematic phase, and i denotes the isotropic phase. This formulation captures the unique mechanical responses associated with molecular alignment in the nematic phase and the disordered structure of the isotropic phase. The parameters used are listed in Table S3. According to the FEA simulation results, the color represents the stress distribution within the actuator, especially between the LCE and the heated film, to ensure that the structure does not fail due to transformation. In addition, the actuator's bending angle has been optimized through controlling the thickness of the LCE layer.

Figure 3E presents the relationship between actuating angle of the LCE actuator and time using 3.7 V voltage for 30 s. For a given voltage, the actuating strain of the LCE actuator elevated initially and afterward attained a plateau due to the temperature distribution in the actuator attained a stable status or due to the fact that the actuation reached its maximum. When the voltage was removed, the actuating recovery rate decreased to 0 in. 4 min. When the voltage was set from 3.7 V, the maximum actuation bending angle was up to 145.06° with a maximum temperature of 130 °C. It took approximately 0.5 min for the LCE actuator to attain the maximal bending angle when 3.7 V was utilized. Our experiments demonstrate that the actuator maintains stable performance over 50 actuation cycles at 3.7 V, with a bending angle variation of less than ±2%. The actuator also exhibits excellent stability, showing negligible degradation after repeated cycling. In addition, no delamination between the LCE tier and the heating film was identified during the cyclical heating and cooling assays. Through fixing the LCE actuator membrane length, we analyzed the actuation driving force of a fixed length with a voltage at 3.7 V for 0.5 min. For a given voltage, the actuation driving force elevated from 0 to the maximal result in 0.5 min and decreased to 0 when the voltage was removed. The maximum actuation driving force elevated from 0 to 99 N when the voltage elevated from 0 to 3.7 V, (Figure S10). An electric-driven LCE actuator, working as an inch worm robot that can crawl down on a slope of 5° with a crawling speed of 7 mm per minute, (see Movie S3), was developed and showcased here.

3.3. Multifunctional Untethered LCE Soft Robot Design, Fabrication, and Characterization. Building upon the aforementioned LCE actuators, we developed a multifunctional, untethered soft robot through the integration of a flexible, PI-substrate based microcontroller (refer to Figure 4A and Figure S11), electronic components such as MOSFETs and wires, a 3.7 V lithium polymer battery, and four LCE actuators. All parts, including heating films (Figure S12), were arranged on the printer platform, and LCE and encapsulating glues were layered and printed directly onto the heating PI films and control board by managing the printing path. Following the completion of printing and curing, a multifunctional, untethered robot was achieved. The heating and cooling of the robot's four legs can be independently controlled via remote control, thereby managing the robot's overall movement. The power consumption of a single heating film is 3.7 W, with the power consumption of the micro-control-unit being negligible. Consequently, the total power consumption of the robot is estimated to be approximately 7.4 W.

In Figure 4B, the untethered robot, equipped with multiple LCE actuators, is shown to be capable of terrestrial locomotion. The robot can walk with a diagonal gait by alternately activating two pairs of actuators for 30 s each. This procedure allows for one pair of actuators to cool as the other pair is activated, enabling diagonal movement. The advantage of this approach is that while one pair of actuators is operational, the other pair can revert to their original shape via cooling, ensuring an uninterrupted power supply and reducing the robot's overall walking time. After conducting tests on the deformation angle and cooling time of a single leg, we set the cooling time for each pair of legs to between 120 s and 150 s to evaluate the robot's speed under different cooling times (Figure 4C and Movie S4). The untethered robot was able to cover approximately 0.2 body lengths (body length: 5.96 cm) per minute after 180 s of movement. When the cooling time was reduced to 120 s, the robot's movement speed increased to 0.28 body lengths per minute.

In subsequent experiments, the robot's movement speed across diverse terrains was assessed (Figure 4D and Movie S5),

https://doi.org/10.1021/acsami.5c06159
ACS Appl. Mater. Interfaces 2025, 17, 36059−36068

as well as its load-bearing capacity on plastic (Figure 4E). These experiments demonstrate the robot's applicability across a variety of environments. The untethered LCE robot's total cost of transport (CoT) is valued at 7 (Supplementary Text 3), significantly lower than previously reported LCE robots (Table 1), dielectric elastomer robots, and SMA robots.[47,48] This reduced CoT can be attributed to the efficiency of the bending actuator structure and the robot's low mass. It is noteworthy that we deliberated between integrating a stretching actuator or a bending actuator into the robot. We ultimately selected the bending actuator design, as it potentially enables a broader range of motions for the same energy consumption.

Furthermore, the untethered robot can function as a soft gripper by adjusting the initial position of the actuators. As depicted in Figure 4F and Movie S6, we demonstrated the ability to create an electronically flexible gripper using an untethered robot to lift various objects. By selectively stimulating the heat wires in each actuator, the gripper could grasp and lift a table tennis ball without additional external control. The heaviest object the soft gripper was able to lift was 14.55 g.

4. CONCLUSION

In this work, we present a comprehensive research methodology for the design, fabrication, and characterization of 4D-printable, LCE-based, and untethered soft robots. The robot used LCE actuators with modifiable LCE materials (with TNI values ranging from 39 to 46 °C) sandwiched between a PI heating film and a silicon adhesive. The electrically responsive LCE actuator-driven untethered soft robot possesses multiple functionalities such as robotic crawling, payload transferring, and adaptive grasping.

The transition temperature adjustable LCE material can be used to circumvent the problem of material deformation difficulty with high transition temperatures, leading to excessive energy expenditure. Moreover, the robot's LCE actuator showcased directional bending from 105.94° to 162.00° at 3.7 V. In contrast to conventional drivers, the driver structure ensured adequate rigidity to support the robot's weight, adequate deformation ability to propel the robot's locomotion, and an optimal packaging structure to prevent LCE and PI separation during heating, thereby eliminating potential failures.

Due to the material improvement and novel structural design, we developed the lightest, quickest untethered electric-driven LCE robot that has the lowest cost of transportation. The weight of the robot was only 9.87 g, crawling at a speed of 0.28 body lengths per minute, and can traverse various terrains and carry objects weighing up to 14.55 g. The cost of transport (CoT) was significantly lower than previous designs (as shown in Table 1).

This untethered LCE robot represents a significant enhancement over previous studies on electrically controlled soft structures, including piezoelectric actuators and SMA driver-based soft robots. While these preceding technologies offer quicker response speeds or greater driving forces, the LCE-based robot operates on low-voltage power, making it compatible with a majority of low-cost, commercially available electronics and batteries. It also features high energy conversion efficiency and remarkably low CoT, critical factors in reducing energy consumption and enhancing the robot's mobility. Its low CoT design allows for smoother and more efficient movement, thus minimizing wear and tear and potentially extending its lifespan.

The advancement of untethered LCE robots may represent a promising progression toward the creation of multifunctional, lightweight, and low-voltage driven soft robots suitable for intricate and unstructured environments. Future endeavors might involve optimizing the LCE actuator's design to achieve superior performance in terms of power consumption and bending angle. Furthermore, research may be conducted to develop LCE-based soft robots with additional functionalities such as wall-climbing and swimming robots. Our LCE actuator-driven, untethered, multifunctional soft robot exemplifies the potential for future developments in soft robotics, where lightweight, adaptable, and versatile robots may find utility across numerous environments, including industrial and domestic applications.

■ ASSOCIATED CONTENT

Data Availability Statement

The data that support the findings of this study are available in the Supporting Information of this article. Supporting information is also available from the Wiley Online Library or from the author.

Supporting Information

The Supporting Information is available free of charge at https://pubs.acs.org/doi/10.1021/acsami.5c06159.

Movie S1: LCE artificial muscle lifting a load (MP4)
Movie S2: Bending actuation of LCE actuator under electrical stimulation (MP4)
Movie S3: Crawling motion of inchworm-inspired LCE robot on a slope (MP4)
Movie S4: Leg movements of untethered LCE soft robot during crawling with varying cooling times (MP4)
Movie S5: Leg movements of untethered LCE soft robot crawling on various surfaces (MP4)
Movie S6: Gripping and lifting of objects by the untethered LCE soft robot (MP4)
Supplementary Texts 1−3 on actuator comparison, FEA modeling, and cost of transport; Figures S1−S13 on material characterization (FTIR, DSC, TGA, DMA, XRD), actuation performance, and robot design; Tables S1−S3 on LCE compositions, robot weights, and model parameters (PDF)

■ AUTHOR INFORMATION

Corresponding Authors

Jianglong Guo − *School of Science, Harbin Institute of Technology (Shenzhen), Shenzhen 518055, People's Republic of China*; Email: guojianglong@hit.edu.cn

Jinsong Leng − *Center for Composite Materials and Structures, Harbin Institute of Technology (HIT), Harbin 150080, People's Republic of China*; orcid.org/0000-0001-5098-9871; Email: lengjs@hit.edu.cn

Authors

Yuliang Xia − *Center for Composite Materials and Structures, Harbin Institute of Technology (HIT), Harbin 150080, People's Republic of China*

Tong Mu − *Center for Composite Materials and Structures, Harbin Institute of Technology (HIT), Harbin 150080, People's Republic of China*

Yanju Liu − *Department of Astronautical Science and Mechanics, Harbin Institute of Technology (HIT), Harbin 150001, People's Republic of China*; orcid.org/0000-0001-8269-1594

Complete contact information is available at: https://pubs.acs.org/10.1021/acsami.5c06159

https://doi.org/10.1021/acsami.5c06159
ACS Appl. Mater. Interfaces 2025, 17, 36059−36068

Author Contributions

†Y.X. and T.M. contributed equally to this work.

Notes

The authors declare no competing financial interest.

■ ACKNOWLEDGMENTS

The authors acknowledge the support by the National Key R&D Program of China (Grant 2022YFB3805700).

■ REFERENCES

(1) Ji, X.; Liu, X.; Cacucciolo, V.; Imboden, M.; Civet, Y.; El Haitami, A.; Cantin, S.; Perriard, Y.; Shea, H. An autonomous untethered fast soft robotic insect driven by low-voltage dielectric elastomer actuators. *Sci. Rob.* **2019**, *4* (37), No. eaaz6451. Accessed Sep 26, 2022.

(2) Rich, S. I.; Wood, R. J.; Majidi, C. Untethered soft robotics. *Nat. Electron.* **2018**, *1* (2), 102−112.

(3) Ze, Q.; Wu, S.; Nishikawa, J.; Dai, J.; Sun, Y.; Leanza, S.; Zemelka, C.; Novelino, L. S.; Paulino, G. H.; Zhao, R. R. Soft robotic origami crawler. *Sci. Adv.* **2022**, *8* (13), No. eabm7834. Accessed Sep 26, 2022.

(4) Ng, C. S. X.; Lum, G. Z. Untethered Soft Robots for Future Planetary Explorations? *Advanced Intelligent Systems* **2023**, *5*, No. 2100106. Accessed Sep 26, 2022.

(5) Chen, S.; Cao, Y.; Sarparast, M.; Yuan, H.; Dong, L.; Tan, X.; Cao, C. Soft Crawling Robots: Design, Actuation, and Locomotion. *Adv. Mater. Technol.* **2020**, *5* (2), No. 1900837. Accessed Jul 11, 2022.

(6) Li, M.; Ostrovsky-Snider, N. A.; Sitti, M.; Omenetto, F. G. Cutting the Cord: Progress in Untethered Soft Robotics and Actuators. *MRS Adv.* **2019**, *4* (51−52), 2787−2804. From Cambridge University Press Cambridge Core.

(7) Ren, Z.; Hu, W.; Dong, X.; Sitti, M. Multi-functional soft-bodied jellyfish-like swimming. *Nat. Commun.* **2019**, *10* (1), 2703.

(8) Dong, Y.; Wang, J.; Guo, X.; Yang, S.; Ozen, M. O.; Chen, P.; Liu, X.; Du, W.; Xiao, F.; Demirci, U.; et al. Multi-stimuli-responsive programmable biomimetic actuator. *Nat. Commun.* **2019**, *10* (1), 4087.

(9) Liu, J. A. C.; Gillen, J. H.; Mishra, S. R.; Evans, B. A.; Tracy, J. B. Photothermally and magnetically controlled reconfiguration of polymer composites for soft robotics. *Sci. Adv.* **2019**, *5* (8), No. eaaw2897. Accessed Sep 26, 2022.

(10) Pilz da Cunha, M.; Ambergen, S.; Debije, M. G.; Homburg, E. F. G. A.; den Toonder, J. M. J.; Schenning, A. P. H. J. A Soft Transporter Robot Fueled by Light. *Adv. Sci.* **2020**, *7* (5), No. 1902842. Accessed Sep 5, 2022.

(11) Qian, X.; Chen, Q.; Yang, Y.; Xu, Y.; Li, Z.; Wang, Z.; Wu, Y.; Wei, Y.; Ji, Y. Untethered Recyclable Tubular Actuators with Versatile Locomotion for Soft Continuum Robots. *Adv. Mater.* **2018**, *30* (29), No. 1801103. Accessed Jul 11, 2022.

(12) Miriyev, A.; Stack, K.; Lipson, H. Soft material for soft actuators. *Nat. Commun.* **2017**, *8* (1), 596.

(13) Kaspar, C.; Ravoo, B. J.; van der Wiel, W. G.; Wegner, S. V.; Pernice, W. H. P. The rise of intelligent matter. *Nature* **2021**, *594* (7863), 345−355.

(14) Ilievski, F.; Mazzeo, A. D.; Shepherd, R. F.; Chen, X.; Whitesides, G. M. Soft Robotics for Chemists. *Angew. Chem., Int. Ed.* **2011**, *50* (8), 1890−1895. Accessed Jul 11, 2022.

(15) Li, M.; Pal, A.; Aghakhani, A.; Pena-Francesch, A.; Sitti, M. Soft actuators for real-world applications. *Nat. Rev. Mater.* **2022**, *7* (3), 235−249.

(16) Laschi, C.; Mazzolai, B.; Cianchetti, M. Soft robotics: Technologies and systems pushing the boundaries of robot abilities. *Sci. Rob.* **2016**, *1* (1), No. eaah3690. Accessed Sep 26, 2022.

(17) Rajappan, A.; Jumet, B.; Preston, D. J. Pneumatic soft robots take a step toward autonomy. *Sci. Rob.* **2021**, *6* (51), No. eabg6994. Accessed Sep 26, 2022.

(18) Tolley, M. T.; Shepherd, R. F.; Mosadegh, B.; Galloway, K. C.; Wehner, M.; Karpelson, M.; Wood, R. J.; Whitesides, G. M. A Resilient, Untethered Soft Robot. *Soft Rob.* **2014**, *1* (3), 213−223. Accessed Sep 26, 2022.

(19) Hu, W.; Lum, G. Z.; Mastrangeli, M.; Sitti, M. Small-scale soft-bodied robot with multimodal locomotion. *Nature* **2018**, *554* (7690), 81−85.

(20) Carrico, J. D.; Hermans, T.; Kim, K. J.; Leang, K. K. 3D-Printing and Machine Learning Control of Soft Ionic Polymer-Metal Composite Actuators. *Sci. Rep.* **2019**, *9* (1), No. 17482.

(21) Xia, Y.; He, Y.; Zhang, F.; Liu, Y.; Leng, J. A Review of Shape Memory Polymers and Composites: Mechanisms, Materials, and Applications. *Adv. Mater.* **2021**, *33* (6), No. 2000713. Accessed Jul 11, 2022.

(22) Pan, X.; Zhang, Y.; Lu, Y.; Yang, F.; Yue, H. A reusable SMA actuated non-explosive lock-release mechanism for space application. *Int. J. Smart Nano Mater.* **2020**, *11* (1), 65−77.

(23) Gu, J.; Zhang, X.; Duan, H.; Wan, M.; Sun, H. A hygro-thermo-mechanical constitutive model for shape memory polymers filled with nano-carbon powder. *Int. J. Smart Nano Mater.* **2021**, *12* (3), 286−306.

(24) Zhao, F.; Zheng, X.; Zhou, S.; Zhou, B.; Xue, S.; Zhang, Y. Constitutive model for epoxy shape memory polymer with regulable phase transition temperature. *Int. J. Smart Nano Mater.* **2021**, *12* (1), 72−87.

(25) Lee, J.-H.; Chung, Y. S.; Rodrigue, H. Long Shape Memory Alloy Tendon-based Soft Robotic Actuators and Implementation as a Soft Gripper. *Sci. Rep.* **2019**, *9* (1), No. 11251.

(26) Kularatne, R. S.; Kim, H.; Boothby, J. M.; Ware, T. H. Liquid crystal elastomer actuators: Synthesis, alignment, and applications. *J. Polym. Sci., Part B: Polym. Phys.* **2017**, *55* (5), 395−411. Accessed Jul 11, 2022.

(27) Ware, T. H.; Biggins, J. S.; Shick, A. F.; Warner, M.; White, T. J. Localized soft elasticity in liquid crystal elastomers. *Nat. Commun.* **2016**, *7* (1), No. 10781.

(28) Qin, B.; Yang, W.; Xu, J.; Wang, X.; Li, X.; Li, C.; Gao, Y.; Wang, Q.-e. Photo-Actuation of Liquid Crystalline Elastomer Materials Doped with Visible Absorber Dyes under Quasi-Daylight. *Polymers* **2020**, *12* (1), 54.

(29) Kotikian, A.; McMahan, C.; Davidson, E. C.; Muhammad, J. M.; Weeks, R. D.; Daraio, C.; Lewis, J. A. Untethered soft robotic matter with passive control of shape morphing and propulsion. *Sci. Rob.* **2019**, *4* (33), No. eaax7044. Accessed Jul 11, 2022.

(30) Zhang, J.; Guo, Y.; Hu, W.; Soon, R. H.; Davidson, Z. S.; Sitti, M. Liquid Crystal Elastomer-Based Magnetic Composite Films for Reconfigurable Shape-Morphing Soft Miniature Machines. *Adv. Mater.* **2021**, *33* (8), No. 2006191. Accessed Sep 26, 2022.

(31) Li, Y.; Yu, H.; Yu, K.; Guo, X.; Wang, X. Reconfigurable Three-Dimensional Mesotructures of Spatially Programmed Liquid Crystal Elastomers and Their Ferromagnetic Composites. *Adv. Funct. Mater.* **2021**, *31* (23), No. 2100338. Accessed Jul 11, 2022.

(32) Ambulo, C. P.; Ford, M. J.; Searles, K.; Majidi, C.; Ware, T. H. 4D-Printable Liquid Metal−Liquid Crystal Elastomer Composites. *ACS Appl. Mater. Interfaces* **2021**, *13* (11), 12805−12813.

(33) Xiao, Y.-Y.; Jiang, Z.-C.; Tong, X.; Zhao, Y. Biomimetic Locomotion of Electrically Powered "Janus" Soft Robots Using a Liquid Crystal Polymer. *Adv. Mater.* **2019**, *31* (36), No. 1903452. Accessed Sep 5, 2022.

(34) Liu, X.; Wei, R.; Hoang, P. T.; Wang, X.; Liu, T.; Keller, P. Reversible and Rapid Laser Actuation of Liquid Crystalline Elastomer Micropillars with Inclusion of Gold Nanoparticles. *Adv. Funct. Mater.* **2015**, *25* (20), 3022−3032. Accessed Jul 11, 2022.

(35) Chen, M.; Gao, M.; Bai, L.; Zheng, H.; Qi, H. J.; Zhou, K. Recent Advances in 4D Printing of Liquid Crystal Elastomers. *Adv. Mater.* **2023**, *35* (23), No. 2209566. Accessed Jun 30, 2023.

(36) He, Q.; Wang, Z.; Wang, Y.; Minori, A.; Tolley, M. T.; Cai, S. Electrically controlled liquid crystal elastomer-based soft tubular actuator with multimodal actuation. *Sci. Adv.* **2019**, *5* (10), No. eaax5746. Accessed Jul 11, 2022.

(37) Boothby, J. M.; Gagnon, J. C.; McDowell, E.; Van Volkenburg, T.; Currano, L.; Xia, Z. An Untethered Soft Robot Based on Liquid Crystal Elastomers. *Soft Rob.* **2022**, *9* (1), 154−162. Accessed Sep 5, 2022.

https://doi.org/10.1021/acsami.5c06159
ACS Appl. Mater. Interfaces 2025, 17, 36059−36068

(38) Cruse, H.; Dürr, V.; Schilling, M.; Schmitz, J. Principles of Insect Locomotion. In *Spatial Temporal Patterns for Action-Oriented Perception in Roving Robots*; Arena, P., Patanè, L., Eds.; Springer: Berlin, 2009; pp 43−96.
(39) Sensenig, A. T.; Shultz, J. W. Mechanics of cuticular elastic energy storage in leg joints lacking extensor muscles in arachnids. *J. Exp. Biol.* **2003**, *206* (4), 771−784. Accessed Jul 4, 2023.
(40) Sydney Gladman, A.; Matsumoto, E. A.; Nuzzo, R. G.; Mahadevan, L.; Lewis, J. A. Biomimetic 4D printing. *Nat. Mater.* **2016**, *15* (4), 413−418.
(41) Schwartz, J. J.; Boydston, A. J. Multimaterial actinic spatial control 3D and 4D printing. *Nat. Commun.* **2019**, *10* (1), 791.
(42) Zhang, W.; Wang, H.; Wang, H.; Chan, J. Y. E.; Liu, H.; Zhang, B.; Zhang, Y.-F.; Agarwal, K.; Yang, X.; Ranganath, A. S.; et al. Structural multi-colour invisible inks with submicron 4D printing of shape memory polymers. *Nat. Commun.* **2021**, *12* (1), 112.
(43) Ceamanos, L.; Kahveci, Z.; López-Valdeolivas, M.; Liu, D.; Broer, D. J.; Sánchez-Somolinos, C. Four-Dimensional Printed Liquid Crystalline Elastomer Actuators with Fast Photoinduced Mechanical Response toward Light-Driven Robotic Functions. *ACS Appl. Mater. Interfaces* **2020**, *12* (39), 44195−44204.
(44) Peng, X.; Wu, S.; Sun, X.; Yue, L.; Montgomery, S. M.; Demoly, F.; Zhou, K.; Zhao, R. R.; Qi, H. J. 4D Printing of Freestanding Liquid Crystal Elastomers via Hybrid Additive Manufacturing. *Adv. Mater.* **2022**, *34*, No. 2204890. Accessed Sep 26, 2022.
(45) Saed, M. O.; Ambulo, C. P.; Kim, H.; De, R.; Raval, V.; Searles, K.; Siddiqui, D. A.; Cue, J. M. O.; Stefan, M. C.; Shankar, M. R.; et al. Molecularly-Engineered, 4D-Printed Liquid Crystal Elastomer Actuators. *Adv. Funct. Mater.* **2019**, *29* (3), No. 1806412. Accessed Oct 13, 2022.
(46) Wang, C.; Sim, K.; Chen, J.; Kim, H.; Rao, Z.; Li, Y.; Chen, W.; Song, J.; Verduzco, R.; Yu, C. Soft Ultrathin Electronics Innervated Adaptive Fully Soft Robots. *Adv. Mater.* **2018**, *30* (13), No. 1706695. Accessed Jul 11, 2022.
(47) Huang, X.; Kumar, K.; Jawed, M. K.; Ye, Z.; Majidi, C. Soft electrically actuated quadruped (SEAQ)—Integrating a flex circuit board and elastomeric limbs for versatile mobility. *IEEE Rob. Autom. Lett.* **2019**, *4* (3), 2415−2422.
(48) Goldberg, B.; Zufferey, R.; Doshi, N.; Helbling, E. F.; Whittredge, G.; Kovac, M.; Wood, R. J. Power and Control Autonomy for High-Speed Locomotion With an Insect-Scale Legged Robot. *IEEE Rob. Autom. Lett.* **2018**, *3* (2), 987−993.
(49) Song, X.; Zhang, W.; Liu, H.; Zhao, L.; Chen, Q.; Tian, H. 3D printing of liquid crystal elastomers-based actuator for an inchworm-inspired crawling soft robot. *Front. Rob. AI* **2022**, *9*, 889848. Original research.

https://doi.org/10.1021/acsami.5c06159
ACS Appl. Mater. Interfaces 2025, 17, 36059−36068